DOI: 10.1002/ejic.200900495

Controllable Synthesis and Luminescence Properties of $La(OH)_3$ and $La(OH)_3:Tb^{3+}$ Nanocrystals with Multiform Morphologies

Guang Jia,[a,b] Yeju Huang,[a,b] Yanhua Song,[a,b] Mei Yang,[a,b] Lihui Zhang,[a,b] and Hongpeng You*[a]

Keywords: Lanthanum / Hydrothermal synthesis / Polymorphism / Luminescence / Nanostructures

One-dimensional $La(OH)_3$ nanocrystals with multiform morphologies have been successfully synthesized by a facile hydrothermal process without using any surfactant, catalyst, or template. It can be found that the pH values of the initial solutions and the alkaline sources play a crucial role in controlling the morphologies of the products. The possible formation process of the 1D samples was investigated in detail. Furthermore, the as-prepared Tb^{3+}-doped $La(OH)_3$ samples show a strong green emission corresponding to $^5D_4$–$^7F_5$ transition of the Tb^{3+} ions under ultraviolet or low-voltage excitation. The experimental results indicate that the luminescence properties of the as-obtained phosphors are dependent on their morphologies and sizes. As a result of the unique luminescence properties and controllable morphology and size, these phosphors may find potential applications in fields such as optoelectronic and nanoscale devices or biological technology.

Introduction

Shape and dimensionality are regarded as particularly important factors that influence the chemical and physical properties of materials. Among the various nanostructures, 1D nanoscaled materials, such as nanowires, nanorods, nanotubes, nanobelts, and so on, have been regarded as significant factors that may bring novel and excellent properties.[1–9] Several strategies have been developed for the growth of 1D nanostructure materials, such as electrochemical methods,[10] template-directed growth technique,[11] vapor–liquid–solid (VLS) synthesis,[12] vapor–solid (VS) method,[13] and hydrothermal process.[1–3,14–17] Among the various synthesis techniques, the hydrothermal process is a powerful method for the fabrication of anisotropic nanomaterials, owing to their great chemical flexibility and synthetic tenability. The advantages of hydrothermal synthesis make it another choice besides the template method. The 1D morphologies of the nanomaterials can usually be controlled by varying the parameters in the reaction system, such as control of reaction temperature and time, change of pH value, and so on.[16–19]

Recently, much research attention has been paid to the synthesis of lanthanide compounds, because they can be used as high-performance phosphors, catalysts, and other functional materials as a result of their novel electronic, optical, and chemical properties arising from their 4f electrons.[2,3,20–24] If rare-earth compounds were fabricated in the form of a 1D nanostructure, they would be expected to be highly functionalized materials, acting as electrically, magnetically, or optically functional host materials as well.[15,25–27] So far, there have been many reports about 1D lanthanide compounds obtained by various synthesis methods.[18,19,28–30] Among them, lanthanum hydroxide [$La(OH)_3$] is of great research interest, and it has been used in many fields, such as catalysis, sorbent materials, high potential oxide ceramics, superconductive materials, hydrogen storage materials, electrode materials, and so on.[31–34] In previous research, 1D $La(OH)_3$ samples, such as nanowires and nanobelts, have been prepared by the hydrothermal method under strongly alkaline conditions.[1,15,31] However, to the best of our knowledge, little has been done on the systematic manipulation of morphologies of uniform and well-dispersed 1D $La(OH)_3$ materials through the simple hydrothermal process under mildly alkaline conditions. Moreover, there have been few reports on lanthanide-ion-doped $La(OH)_3$ luminescent materials.

Herein, we report the controllable synthesis of 1D $La(OH)_3$ materials with various morphologies through a simple solution-based hydrothermal process without using any catalyst or template. The morphologies of the products could be modulated by simply adjusting the pH values of

[a] State Key Laboratory of Rare Earth Resource Utilization, Changchun Institute of Applied Chemistry, Chinese Academy of Sciences,
Changchun 130022, P. R. China
E-mail: hpyou@ciac.jl.cn
[b] Graduate University of the Chinese Academy of Sciences, Beijing 100049, P. R. China

Supporting information for this article is available on the WWW under http://dx.doi.org/10.1002/ejic.200900495.

the initial solution or by using different kinds of alkaline sources. Furthermore, the photoluminescence (PL) and cathodoluminescence (CL) properties of the $La(OH)_3:Tb^{3+}$ green phosphors have been discussed in detail.

Results and Discussion

Figure 1a,b shows the XRD patterns of the $La(OH)_3$ samples prepared at pH 7 and 9 by using ammonia as the alkaline source. It can be seen that the diffraction peaks of the two samples can be well indexed to the hexagonal phase of $La(OH)_3$ (JCPDS No. 36-1481). The calculated lattice constants ($a = b = 6.525$ Å, $c = 3.843$ Å) using the Jade 5.0 program for the sample prepared at pH 9 are compatible with the standard card (JCPDS No. 36-1481; $a = b = 6.529$ Å, $c = 3.859$ Å). When the reaction was performed by using a mixture of ammonia and hydrazine hydrate ($N_2H_4 \cdot H_2O$) or pure hydrazine hydrate as the alkaline source, the diffraction peaks of the samples also agree well with the pure phase of hexagonal $La(OH)_3$ (JCPDS No. 36-1481; Figure 1c,d). It is worth pointing out that the XRD patterns also indicate that there is a large difference from each other in the relative intensities based on (110), (100), and (101) peaks for the samples, indicating the possibility of different preferential growth orientations under different pH conditions or alkaline sources.

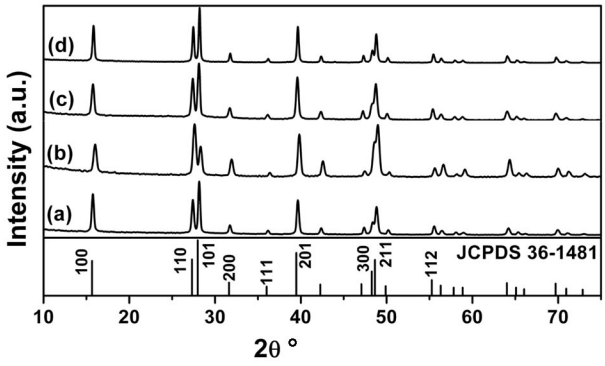

Figure 1. XRD patterns of the samples with ammonia as alkaline source at (a) pH 7 and (b) pH 9 and with (c) a mixture of ammonia and hydrazine hydrate and (d) pure hydrazine hydrate as alkaline sources at pH 9. The standard data for hexagonal phase $La(OH)_3$ (JCPDS No. 36-1481) is also presented in the figure for comparison.

Figure 2 is a panoramic SEM image of the $La(OH)_3$ sample prepared at pH 9 (ammonia as alkaline sources), clearly indicating that the as-formed $La(OH)_3$ product consists of nanowires in 100% morphological yield. The nanowires display uniform morphology with diameters of 40–50 nm and lengths up to several micrometers. As seen from the magnified SEM image (Figure 2b), the uniform nanowires are straight and their surfaces are very smooth. In addition, the $La(OH)_3$ sample was further examined by transmission electron microscopy. Figure 2c shows a typical TEM image of the $La(OH)_3$ sample, clearly exhibiting that the sample is entirely composed of uniform nanowires with diameters of 40–50 nm, which is consistent with the result shown in the SEM images (Figure 2a,b). Figure 2d shows a typical high-magnification TEM image of a single $La(OH)_3$ nanowire. The corresponding SAED pattern (Figure 2d, inset) taken from this nanowire reveals the single-crystalline nature with a typical hexagonal structure.

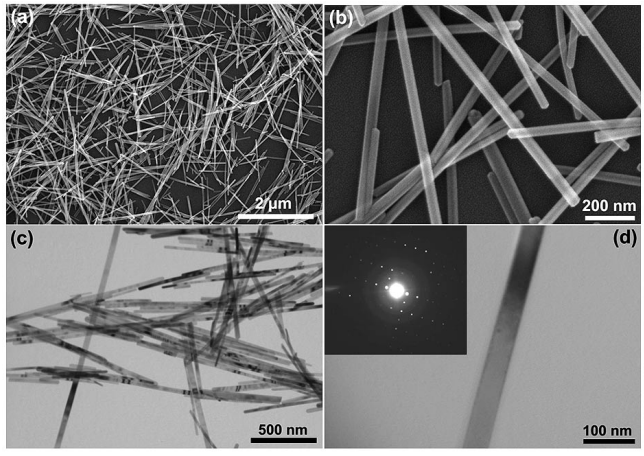

Figure 2. (a) Low- and (b) high-magnification SEM images, and (c) TEM image of the $La(OH)_3$ samples prepared at pH 9 with ammonia as alkaline source. (d) TEM image of a single nanowire (inset in d is the corresponding SAED pattern taken from the nanowire).

Time-independent experiments were preformed to investigate the crystal growth of the uniform 1D nanowires (200 °C, pH 9). Adjustment of the pH value of the solution led to the formation of $La(OH)_3$ nanowires with poor crystallinity before hydrothermal treatment. By increasing the hydrothermal reaction time, the morphology and size of the $La(OH)_3$ samples did not change obviously, but the surface of the nanowires became smoother (Supporting Information, Figure S1). In addition, $La(OH)_3$ nanowires with higher crystallinity can be obtained with an increase in the reaction time. This is important for phosphors, because high crystallinity generally means less traps and stronger luminescence. This result can be confirmed by the XRD patterns of the $La(OH)_3$ samples prepared at different time (Supporting Information, Figure S2).

The pH values of the colloidal solution have great effects on the size and morphology of the hydrothermal products. The wide-field SEM image (Supporting Information, Figure S3a) of $La(OH)_3$ sample prepared at pH 7 shows that the sample is composed of nanorods with diameters of 50–60 nm and lengths in the range 300–500 nm. The magnified SEM image of the product (Figure 3a) indicates that the nanorods are very straight and their surfaces are smooth. The $La(OH)_3$ sample prepared at pH 10 is composed of uniform nanobundles with diameters of about 200 nm and lengths in the range 1–1.5 μm (Supporting Information, Figure S3b). The enlarged SEM image indicates that the nanobundles consist of individual parallel nanowires with diameters of about 30 nm (Figure 3b). As seen from the SEM and TEM observations mentioned above, 1D $La(OH)_3$ materials with various morphologies can be obtained by simply adjusting the pH values of the initial solution.

The morphological evolution of the samples can be ascribed to the change in the chemical potential in solution. When the pH value of the initial solution increased from 7 to 9, the mean aspect ratio of the sample increased dramatically. A higher pH value implies a higher OH^- ion concentration and a higher chemical potential in solution. Consequently, the nucleating process occurred faster and more nuclei of crystals formed, resulting in the high aspect ratio of the samples. By increasing the pH value to 10, the nanowires self-assembled into bundles along their cross-sectional diameter through a direct aggregation growth process, which was probably because the crystal facets along the cross-sectional diameter matched well, offering a low surface energy.[1,19,34,35]

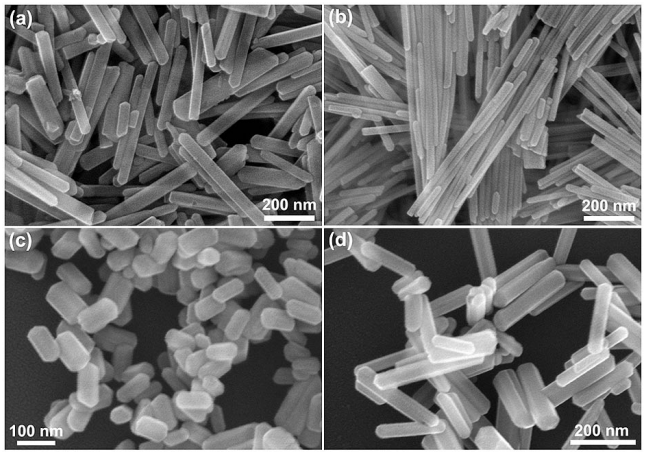

Figure 3. SEM images of the $La(OH)_3$ samples prepared at (a) pH 7 and (b) pH 10 with ammonia as alkaline source and (c) at pH 9 with pure hydrazine hydrate and (d) a mixture of ammonia and hydrazine hydrate as alkaline sources.

The alkaline sources of the initial reaction solutions have great effects on the morphologies of the final products. Figure 3c,d show the typical SEM images for $La(OH)_3$ sample prepared at pH 9 by using hydrazine hydrate ($N_2H_4{\cdot}H_2O$) as alkaline source. As can be seen from a low-magnification SEM image (Supporting Information, Figure S3c), the as-prepared sample is almost entirely composed of short hexagonal nanoprisms with perfect uniformity and well-defined crystallographic facets. Analysis of a number of the nanoprisms shows that these hexagonal prisms have average diameters of about 50 nm and lengths of about 100 nm. Furthermore, from the images of a higher magnification (Figure 3c), it can be observed that these nanoprisms have clear edges and smooth side planes. Compared with the samples prepared by ammonia at pH 9 (Figure 2), the as-obtained hexagonal nanoprisms have no obvious change in diameter, whereas the lengths of the particles decrease remarkably from several micrometers to about 100 nm. In comparison, the experiments were carried out by using a mixture of ammonia and hydrazine hydrate as alkaline sources (pH 9). One can clearly see that the as-obtained sample consists of uniform hexagonal nanoprisms with higher aspect ratios (Supporting Information, Figure S3d). The magnified SEM image (Figure 3d) exhibits that the hexagonal nanoprisms have diameters of about 50 nm and lengths of 200–300 nm. It can be concluded that the aspect ratios of the samples reduces with an increase in the concentration of $N_2H_4{\cdot}H_2O$. On the basis of the above SEM observations, we can assume that hydrazine hydrate may have dual functions in the formation process of $La(OH)_3$ samples. One role is to function as alkaline source in the solution for the formation of $La(OH)_3$. The other is that hydrazine hydrate may act as crystal facet inhibitors in the system. In the process, the hydrazine hydrate may be selectively absorbed on specific crystal facets of the initial $La(OH)_3$ crystals and change the growth rates of different facets, resulting in the formation of the hexagonal prismatic geometries of the $La(OH)_3$ crystals. In addition, the hydrazine hydrate may be preferentially absorbed on the surfaces that are perpendicular to the intrinsic growing directions of the hexagonal $La(OH)_3$, resulting in a decrease in the aspect ratios with an increase in the concentration of $N_2H_4{\cdot}H_2O$ in the initial solution (Figures 2 and 3). The result can be confirmed by the FTIR spectra of the as-obtained $La(OH)_3$ nanowires and nanoprisms (Figure 4). For the $La(OH)_3$ nanowires, the bands centered at 3610 and 3423 cm^{-1} can be attributed to the O–H vibrations of the OH^- ions and the absorbed water of the $La(OH)_3$ sample. The band at about 648 cm^{-1} is assigned to the La–O stretching frequencies of $La(OH)_3$. The absorption bands at 1509 and 1369 cm^{-1} are ascribed to N–H vibrations of the amino groups, which may be caused by the absorbed NH_3 molecules during the hydrothermal process. The FTIR spectral profile of $La(OH)_3$ nanoprisms is similar to that of the $La(OH)_3$ nanowires. More importantly, it can be observed that the absorption intensity of the N–H vibrations for nanoprisms is much stronger than that of the $La(OH)_3$ nanowires, which indicates that much more N_2H_4 molecules have been absorbed in the $La(OH)_3$ nanoprisms. The result can effectively support the hypothesis for the influence of $N_2H_4{\cdot}H_2O$ during the hydrothermal reaction.

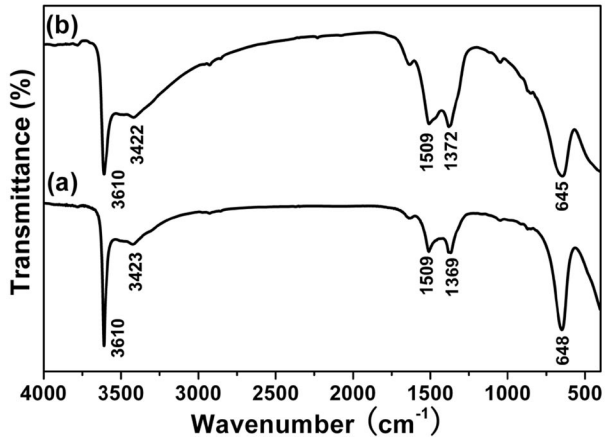

Figure 4. FTIR spectra of the $La(OH)_3$ (a) nanowires and (b) nanoprisms.

The Tb^{3+}-doped $La(OH)_3$ samples were prepared to investigate the luminescence properties. We can see that all the Tb^{3+}-doped $La(OH)_3$ samples exhibit the peaks of pure hexagonal $La(OH)_3$ (JCPDS No. 36-1481; Supporting Information, Figure S4). We can also observe that the diffraction peaks shift to higher angle side gradually with an increase in the doping concentration of Tb^{3+}. Take $La(OH)_3$: 2%Tb^{3+} as an example: the calculated lattice constants ($a = b = 6.493$ Å, $c = 3.841$ Å) are a little smaller than those of the undoped sample ($a = b = 6.525$ Å, $c = 3.843$ Å). These results indicate that the Tb^{3+} ions with smaller radii have been effectively doped into the $La(OH)_3$ host lattice. The energy dispersive X-ray spectrum (EDX) was further used to investigate the as-obtained $La(OH)_3$:Tb^{3+} sample. The EDX spectrum (Supporting Information, Figure S5) confirms the presence of lanthanum (La), terbium (Tb), and oxygen (O) elements in the $La(OH)_3$:Tb^{3+} sample. No other impurity peaks can be detected, which can effectively support the XRD results of the sample.

The as-obtained $La(OH)_3$:Tb^{3+} samples exhibit a strong green emission under short ultraviolet irradiation, and the spectral properties are similar to those of other Tb^{3+}-doped luminescent materials.[36–39] The excitation spectrum of the $La(OH)_3$:Tb^{3+} nanowires (Figure 5a) is composed of a broad band centered at 240 nm and some sharp bands in the region from 275 to 400 nm. The broad band and small peaks at 275 and 289 nm are ascribed to the spin-allowed and spin-forbidden interconfigurational $4f^8$–$4f^75d^1$ transition of the Tb^{3+} ions, respectively. In the longer wavelength region (from 310 to 400 nm), the sharp bands correspond to absorption of the forbidden f–f transitions of the Tb^{3+} ions. Upon excitation at 240 nm, the emission spectra (Figure 5b) of the $La(OH)_3$:2%Tb^{3+} phosphors consist of a group of lines centered at about 491, 544, 584, and 620 nm, which corresponds to the $^5D_4$–^7F_J, ($J = 6, 5, 4, 3$) transitions of the Tb^{3+} ions, respectively. The dominant emission band is located at 544 nm, which is a typical green band caused by the $^5D_4$–$^7F_5$ transition of the Tb^{3+} ions. As we know, the morphology and size of the lanthanide-base luminescent materials cannot influence the typical line spectra on the basis of intra-4f transitions, but may affect the emission intensity as a result of the change in their specific surface area.[18,34,40] From the comparative emission spectra of the as-obtained $La(OH)_3$:2%Tb^{3+} nanowires (ammonia as alkaline source) and the short hexagonal nanoprisms (hydrazine hydrate as alkaline source), it can be seen that the two samples show similar spectral patterns without any emission band shift, but one can clearly observe that the nanowire phosphor has a higher PL intensity than nanoprism phosphor. It is well known that the surface area of materials increases along with a decrease in size. The large surface area introduces a large number of defects into the phosphor crystal, which have a serious drawback on the PL intensity of the phosphors. If the surface area is greatly reduced, which results from increased crystallite size, the phosphor with fewer defects would show great improvement in PL intensity.[18,34,40] From the SEM and TEM results presented above (Figures 2 and 3), it can be observed that the surface area of the $La(OH)_3$ nanowires is lower than that of the nanoprisms. This result can be confirmed by BET measurements of the as-obtained $La(OH)_3$ samples (Figure 6). The specific surface areas of the $La(OH)_3$ nanowires and nanoprisms were calculated to be 103.9 and 118.3 $m^2 g^{-1}$, respectively. Furthermore, it can be seen from the FTIR spectra that a large number of hydrazine hydrate molecules were adsorbed onto the surface of the $La(OH)_3$ nanoprisms. They would have an effect on the formation of surface defects (PL killer sites), which might decrease the PL intensity and shorten the PL lifetime. This result can also be confirmed by the decay curves of the two samples (Supporting Information, Figure S7).

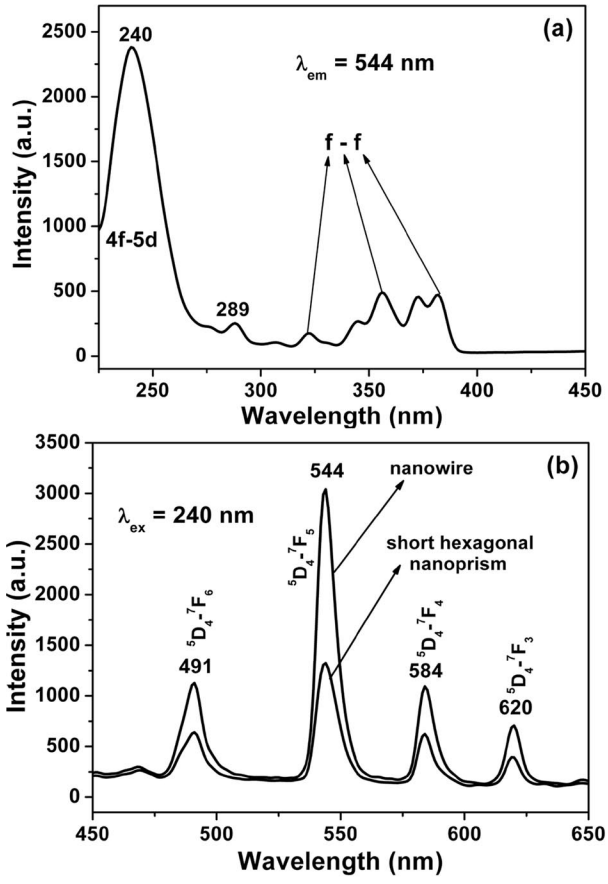

Figure 5. (a) Excitation and (b) emission spectra of $La(OH)_3$: 2%Tb^{3+} samples with different shapes under excitation at 240 nm.

As we know, the PL intensity of the phosphor is strongly influenced by the activator concentration.[41–43] The PL intensities for the emission spectra clearly vary with changes in the Tb^{3+}-doping concentration. As shown in Figure S6 (Supporting Information), the PL intensity first increases with an increase in the activator concentration, reaching a maximum value at 2%, and then decreases with a further increase in the doping concentration. It is well known that the PL intensity is related to the average distance between luminescent centers. As the doping concentration of the activator ions increases, the distance between active ions decreases. The interaction between active ions will cause concentration quenching when the distance is short enough.

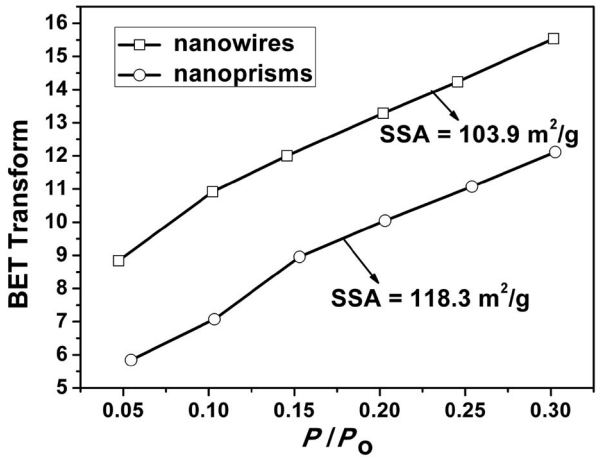

Figure 6. BET surface area of La(OH)$_3$ nanowires and nanoprisms.

The luminescence decay curves for the luminescence of Tb^{3+} ions (544 nm, $^5D_4$–$^7F_5$ transition) in the host lattices of La(OH)$_3$:2%Tb^{3+} nanowires and nanoprisms were investigated (Supporting Information, Figure S7). The decay curves can be well fitted into a single-exponential function as $I = A[\exp(-t/\tau)]$, and the lifetimes of the Tb^{3+} ions were determined to be 1.289 and 1.218 ms for nanowires and nanoprisms, respectively. The result is basically in agreement with other Tb^{3+}-doped phosphors in previous reports.[37,44,45]

The CL properties of the as-obtained La(OH)$_3$:2%Tb^{3+} phosphors were also investigated. Figure 7 shows typical CL spectra of the La(OH)$_3$:Tb^{3+} nanowires and short nanoprisms under the excitation of an electron beam (accelerating voltage = 3 kV; filament current = 98 mA). It can be seen that the as-prepared La(OH)$_3$:Tb^{3+} phosphors exhibit strong green emission under low-voltage excitation. The peak positions of the emission peaks are similar to those of the emission spectra in Figure 5b. However, the relative intensity of the peaks in the PL and CL spectra varies obviously, which may be caused by the different excitation

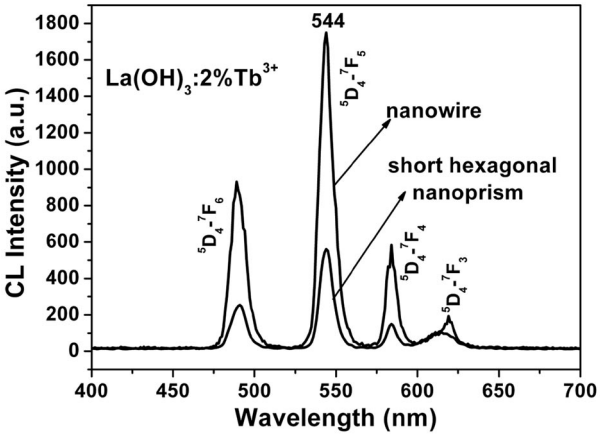

Figure 7. Typical cathodoluminescence spectra of La(OH)$_3$:2%Tb^{3+} phosphors excited by a low-voltage electron beam (accelerating voltage = 3 kV; filament current = 98 mA).

mechanism. In addition, we can observe that the CL intensity of La(OH)$_3$:Tb^{3+} nanowires is much higher than that of the nanoprisms. This result is in good accordance with the PL spectra presented above (Figure 5b).

Conclusions

In summary, the controllable synthesis of 1D La(OH)$_3$ samples with different morphologies (such as nanowires, nanorods, nanobundles, and nanoprisms) has been successfully achieved through a simple hydrothermal method. The morphology, crystal structure, and luminescence properties of the samples have been investigated in detail. The morphologies of the products can be modulated by simply adjusting the pH values or by using different kinds of alkaline sources. The experimental results indicate that the luminescence properties of the as-obtained phosphors are dependent on their morphologies and sizes. The uniform, dispersed, and homogeneous La(OH)$_3$:Tb^{3+} phosphors may be potentially applied in optoelectronic and nanoscale devices or biological technology. Furthermore, this general and simple method may be of much significance in the synthesis of many other 1D hydroxides and oxides with multiform morphologies.

Experimental Section

General: The rare-earth oxides La_2O_3 (99.99%) and Tb_4O_7 (99.99%) were purchased from Wuxi Yiteng Rare-Earth Limited Corporation (China), and other chemicals were purchased from Beijing Chemical Corporation. All chemicals were of analytical grade and used directly without further purification.

Preparation: La(NO$_3$)$_3$ and Tb(NO$_3$)$_3$ aqueous solutions were obtained by dissolving La_2O_3 (99.99%) and Tb_4O_7 (99.99%) in dilute HNO_3 solution under heating with agitation. In a typical synthesis, an aqueous solution of La(NO$_3$)$_3$ (1 M, 2 mL) was added to deionized water (35 mL). Then, an ammonia solution (25 wt.-%) was introduced rapidly into the vigorously stirred solution until pH 9. After additional agitation for 1 h, the as-obtained white colloidal suspension was transferred to a 50-mL autoclave, sealed, and heated at 200 °C for 24 h. The autoclave was then cooled to room temperature naturally. The product was washed with deionized water and absolute ethanol several times, and dried at 60 °C in air. Other samples were prepared by a similar procedure, except for different pH conditions (7, 10) or alkaline source (hydrazine hydrate).

In order to investigate the luminescence of the La(OH)$_3$ products, the Tb^{3+}-doped La(OH)$_3$ samples were prepared by introducing a proper amount of Tb(NO$_3$)$_3$ solution instead of La(NO$_3$)$_3$ into the initial solution as described above.

Characterization: The samples were characterized by powder X-ray diffraction (XRD) performed with a D8 Focus diffractometer (Bruker). The morphology and composition of the samples were inspected by using a scanning electron microscope (SEM; S-4800, Hitachi) equipped with an energy-dispersive X-ray spectrum (EDX; XFlash-Detector 4010, Bruker). Transmission electron microscopy (TEM) images and selected-area electron diffraction (SAED) patterns were obtained by using a JEOL 2010 transmission electron microscope operating at 200 kV. Fourier transform infra-

red spectroscopy (FTIR) spectra were measured with a Perkin–Elmer 580B infrared spectrophotometer as KBr pellets. Specific surface area was calculated by the Brunauer-Emmett-Teller (BET) method by using adsorption isotherms with N_2 as the adsorbate at liquid nitrogen temperatures. Photoluminescence (PL) excitation and emission spectra were recorded with a Hitachi F-4500 spectrophotometer equipped with a 150 W xenon lamp as the excitation source. The cathodoluminescence (CL) measurements were carried out in an ultrahigh-vacuum chamber ($<10^{-8}$ Torr), where the samples were excited by a low-voltage electron beam (accelerating = 3 kV; filament currents = 98 mA), and the spectra were recorded with an F-4500 spectrophotometer. The luminescence decay curves were obtained from a Lecroy Wave Runner 6100 Digital Oscilloscope (1 GHz) using a tunable laser (pulse width = 4 ns, gate = 50 ns) as the excitation (Contimuum Sunlite OPO). All measurements were performed at room temperature.

Supporting Information (see footnote on the first page of this article): SEM images and XRD patterns of the $La(OH)_3$; low-magnification SEM images of the $La(OH)_3$ samples; XRD patterns, EDX spectrum, emission intensity, and decay curves of $La(OH)_3:Tb^{3+}$ nanowires.

Acknowledgments

This work was financially supported by the National Natural Science Foundation of China (Grant No. 20771098) and the National Basic Research Program of China (973 Program, Grant No. 2007CB935502).

[1] X. Wang, Y. D. Li, *Angew. Chem. Int. Ed.* **2002**, *41*, 4790–4793.
[2] J. L. Zhuang, L. F. Liang, H. Sung, X. F. Yang, M. M. Wu, I. D. Williams, S. H. Feng, Q. Su, *Inorg. Chem.* **2007**, *46*, 5404–5410.
[3] L. F. Liang, H. F. Xu, Q. Su, H. Konishi, Y. B. Jiang, M. M. Wu, Y. F. Wang, D. Y. Xia, *Inorg. Chem.* **2004**, *43*, 1594–1596.
[4] J. M. Wang, L. Gao, *J. Mater. Chem.* **2003**, *13*, 2551–2554.
[5] J. Nishijo, O. Oishi, K. Judai, N. Nishi, *Chem. Mater.* **2007**, *19*, 4627–4629.
[6] M. H. Huang, S. Mao, H. Feick, H. Yan, Y. Wu, H. Kind, E. Weber, R. Russo, P. D. Yang, *Science* **2001**, *292*, 1897–1899.
[7] Y. N. Xia, P. D. Yang, Y. G. Sun, Y. Y. Wu, B. Mayers, B. Gates, Y. D. Yin, F. Kim, H. Q. Yan, *Adv. Mater.* **2003**, *15*, 353–389.
[8] L. Zhao, T. Lu, M. Yosef, M. Steinhart, M. Zacharias, U. Gosele, S. Schlecht, *Chem. Mater.* **2006**, *18*, 6094–6096.
[9] B. Wang, L. F. Zhu, Y. H. Yang, N. S. Xu, G. W. Yang, *J. Phys. Chem. C* **2008**, *112*, 6643–6647.
[10] D. Xu, Y. Xu, D. Chen, G. Guo, L. Gui, Y. Tang, *Adv. Mater.* **2000**, *12*, 520–523.
[11] M. Yada, M. Mihara, S. Mouri, M. Kuroki, T. Kijima, *Adv. Mater.* **2002**, *14*, 309–313.
[12] X. F. Duan, C. M. Lieber, *Adv. Mater.* **2000**, *12*, 298–302.
[13] Z. W. Pan, Z. R. Dai, Z. L. Wang, *Science* **2001**, *291*, 1947–1949.
[14] G. P. Patzke, F. Krumeich, R. Nesper, *Angew. Chem. Int. Ed.* **2002**, *41*, 2446–2461.
[15] X. Wang, Y. D. Li, *Chem. Eur. J.* **2003**, *9*, 5627–5635.
[16] X. Wang, Y. D. Li, *Inorg. Chem.* **2006**, *45*, 7522–7534.
[17] G. F. Zou, H. Li, Y. G. Zhang, K. Xiong, Y. T. Qian, *Nanotechnology* **2006**, *17*, S313–S320.
[18] J. Yang, C. X. Li, Z. Y. Cheng, X. M. Zhang, Z. W. Quan, C. M. Zhang, J. Lin, *J. Phys. Chem. C* **2007**, *111*, 18148–18154.
[19] J. Zhang, Z. Liu, J. Lin, J. Fang, *Cryst. Growth Des.* **2005**, *5*, 1527–1530.
[20] M. S. Palmer, M. Neurock, M. M. Olken, *J. Am. Chem. Soc.* **2002**, *124*, 8452–8461.
[21] W. H. Di, X. J. Wang, B. J. Chen, H. S. Lai, X. X. Zhao, *Opt. Mater.* **2005**, *27*, 1386–1390.
[22] J. P. Cotter, J. C. Fitzmaurice, I. P. Parkin, *J. Mater. Chem.* **1994**, *4*, 1603–1609.
[23] G. Jia, M. Yang, Y. H. Song, H. P. You, H. J. Zhang, *Cryst. Growth Des.* **2009**, *9*, 301–307.
[24] A. H. Peruski, L. H. Johnson, L. F. Peruski, *J. Immunol. Methods* **2002**, *263*, 35–41.
[25] C. G. Hu, H. Liu, W. T. Dong, Y. Y. Zhang, G. Bao, C. S. Lao, Z. L. Wang, *Adv. Mater.* **2007**, *19*, 470–474.
[26] R. X. Yan, X. M. Sun, X. Wang, Q. Peng, Y. D. Li, *Chem. Eur. J.* **2005**, *11*, 2183–2195.
[27] Y. P. Fang, A. W. Xu, R. Q. Song, H. X. Zhang, L. P. You, J. C. Yu, H. Q. Liu, *J. Am. Chem. Soc.* **2003**, *125*, 16025–16034.
[28] G. Wang, Z. D. Wang, Y. X. Zhang, G. T. Fei, L. D. Zhang, *Nanotechnology* **2004**, *15*, 1307–1311.
[29] A. W. Xu, Y. P. Fang, L. P. You, H. Q. Liu, *J. Am. Chem. Soc.* **2003**, *125*, 1494–1495.
[30] C. K. Chang, Q. A. Zhang, D. L. Mao, *Nanotechnology* **2006**, *17*, 1981–1985.
[31] F. Niu, A. M. Cao, W. G. Song, L. J. Wan, *J. Phys. Chem. C* **2008**, *112*, 17988–17993.
[32] J. L. Zhu, Y. H. Zhou, H. X. Yang, *J. Power Sources* **1997**, *69*, 169–173.
[33] M. P. Rosynek, D. T. Magnuson, *J. Catal.* **1977**, *46*, 402–413.
[34] B. Tang, J. C. Ge, L. H. Zhuo, *Nanotechnology* **2004**, *15*, 1749.
[35] Q. Tang, Z. P. Liu, S. Li, S. Y. Zhang, X. M. Liu, Y. T. Qian, *J. Cryst. Growth* **2003**, *259*, 208–214.
[36] H. P. You, G. Y. Hong, X. Y. Wu, J. K. Tang, H. P. Hu, *Chem. Mater.* **2003**, *15*, 2000–2004.
[37] M. Yu, H. Wang, C. K. Lin, G. Z. Li, J. Lin, *Nanotechnology* **2006**, *17*, 3245–3252.
[38] Y. X. Zhang, S. S. Pan, X. M. Teng, Y. Y. Luo, G. H. Li, *J. Phys. Chem. C* **2008**, *112*, 9623–9626.
[39] J. C. Boyer, J. Gagnon, L. A. Cuccia, J. A. Capobianco, *Chem. Mater.* **2007**, *19*, 3358–3360.
[40] J. X. Wan, Z. H. Wang, X. Y. Chen, L. Mu, Y. T. Qian, *J. Cryst. Growth* **2005**, *284*, 538–543.
[41] M. Yu, J. Lin, Z. Wang, J. Fu, S. Wang, H. J. Zhang, Y. C. Han, *Chem. Mater.* **2002**, *14*, 2224–2231.
[42] K. B. Kim, Y. I. Kim, H. G. Chun, T. Y. Cho, J. S. Jung, J. G. Kang, *Chem. Mater.* **2002**, *14*, 5045–5052.
[43] K. Y. Jung, H. W. Lee, H. K. Jung, *Chem. Mater.* **2006**, *18*, 2249–2255.
[44] X. M. Zhang, J. H. Zhang, L. F. Liang, Q. Su, *Mater. Res. Bull.* **2005**, *40*, 281–288.
[45] Q. Y. Zhang, K. Pita, W. Ye, W. X. Que, *Chem. Phys. Lett.* **2002**, *351*, 163–170.

Received: June 3, 2009
Published Online: July 23, 2009

